

Geometrical Frustration and Cluster Spin Glass with Random Graphs

Alexandre Silveira, R. Erichsen Jr., and S. G. Magalhães
*Instituto de Física, Universidade Federal do Rio Grande do Sul,
Caixa Postal 15051,91501-970 Porto Alegre, RS, Brazil*

(Dated: December 7, 2021)

Abstract

We develop a novel method based in the sparse random graph to account the interplay between geometric frustration and disorder in cluster magnetism. Our theory allows to introduce the cluster network connectivity as a controllable parameter. Two types of inner cluster geometry are considered: triangular and tetrahedral. The theory was developed for a general, non-uniform intra-cluster interactions, but in the present paper the results presented correspond to uniform, anti-ferromagnetic (AF) intra-clusters interactions J_0/J . The clusters are represented by nodes on a finite connectivity random graph, and the inter-cluster interactions are random Gaussian distributed. The graph realizations are treated in replica theory using the formalism of order parameter functions, which allows to calculate the distribution of local fields and, as a consequence, the relevant observable. In the case of triangular cluster geometry, there is the onset of a classical Spin Liquid state at a temperature T^*/J and then, a Cluster Spin Glass (CSG) phase at a temperature T_f/J . The CSG ground state is robust even for very weak disorder or large negative J_0/J . These results does not depend on the network connectivity. Nevertheless, variations in the connectivity strongly affect the level of frustration $f_p = -\Theta_{CW}/T_f$ for large J_0/J . In contrast, for the non-frustrated tetrahedral cluster geometry, the CSG ground state is suppressed for weak disorder or large negative J_0/J . The CSG boundary phase presents a re-entrance which is dependent on the network connectivity.

I. INTRODUCTION

Magnetism in clusters of spins is a very promising novel frontier both in terms of fundamental physics and applications [1]. The starting point is that the spins cluster is a structure with constituent elements such as inner geometry, chemical composition and size, whose combined effects makes cluster magnetism full of possibilities for new magnetic materials.

One of them, still little explored, is the relationship between cluster magnetism and geometrical frustration (GF) [2]. This concept has been a central topic in condensed matter physics [3]. More recently, its presence has been understood as the cornerstone for the existence of exotic states of matter, such as classical or quantum spin-liquids (SL) [4]. It should be noted that this relationship may have also technological interest, since frustration may be behind a significant increase in the magnetocaloric effect [5, 6].

The question is: how to contact cluster magnetism with GF? Our answer is based on the assumption that, in cluster magnetism, the spin lattice is replaced by a spin cluster network. From that point, if there is disorder also present, we follow the main assumptions of the cluster mean field (CMF) theory for spin glasses [7, 8]. Firstly, one consider that spin clusters themselves can interact rather than individual spins. This is a situation similar to what has already been proposed for nanomagnetism (see, for instance, [9]). Next, the problem is separated into intra and inter-cluster parts which are self consistently coupled leading to the glassy instability. The effects of the GF can come from the intra-cluster part considering, for instance, a suitable inner cluster geometry with, for instance, anti-ferromagnetic (AF) interactions.

Indeed, such approach allowed to obtain non-trivial results [10–12]. For instance, in the case of Ising spins using the kagome geometry, it is introduced a novel mechanism to stabilize a cluster spin glass (CSG) phase at low temperature with much

weaker disorder compared to that one required for individual spins. This mechanism is related to the formation of a region with a classical spin-liquid (SL) given by a plateau in the entropy at lower temperatures which precedes the CSG instability. We highlight that this behaviour is observed in real systems (see [13–15]).

Nevertheless, the CMF theory assumes that the cluster network is fully connected. Such assumption may lead to an inadequate account for the GF within the self-consistent procedure which couples the intra and inter-cluster parts. Thus, one should evaluate properly whether and how the variation in the connectivity of the cluster network can affect the self-consistency and, therefore, the GF effects in the disordered cluster magnetism.

In this paper, we propose to study of the CSG state in a random graph architecture with finite connectivity. The main reason to adopt this architecture is that, since it allows to control the network connectivity, it is more realistic than the fully connected network mean field approach. We apply it for triangular and tetrahedral clusters with uniform AF intra-cluster interactions, in order to compare results with and without GF effects.

In order to deal with the realizations of the random network, we use the replica theory [16, 17], that consist in rewriting the replicated partition function in terms of order parameter functions and then taking the replica limit. The order parameter functions are then parameterized in terms of a local field distribution, which is self consistently calculated through a population dynamics algorithm. It is well known that bellow the spin glass transition, replica symmetry is broken. The instability of the replica symmetry solution is obtained through the two-replica method [18].

There are other methods to deal with the finite connectivity random network, such as the cavity method [19]. The equations of the cavity method are written down considering an unique realization of the network disorder, but it becomes equivalent to the replica method when the disorder average is performed. Here, we focus mainly in

the replica symmetry (RS) theory. The development of a replica symmetry breaking (RSB) theory for the cluster network with finite connectivity, to deal with geometric frustration effects, is beyond the objective of this paper.

The paper is organized as follows. In Sec. II we derive the equations for the model using the replica method. In Sec. III we present the results characterizing the system by drawing phase diagrams for the thermodynamic phases. The conclusions and other remarks are found in section IV.

II. MODEL AND REPLICA PROCEDURE

We study a system of N_{cl} interacting clusters. The Ising spins that belong to each cluster can assume the values $\sigma_{\mu i} = \pm \frac{1}{2}$, where $\mu = 1 \dots N_{cl}$ is the cluster index and $i = 1 \dots p$ is the intra-cluster index. The inter-cluster interaction $J_{\mu\nu}$ is chosen from a Gaussian distribution with mean zero and variance J^2 . The Hamiltonian of this system is given by

$$H(\boldsymbol{\sigma}) = -\frac{1}{\sqrt{c}} \sum_{\mu < \nu} c_{\mu\nu} J_{\mu\nu} \sigma_{\mu} \sigma_{\nu} - \theta \sum_{\mu} \sigma_{\mu} + \sum_{\mu} H_0(\boldsymbol{\sigma}_{\mu}) \quad (1)$$

where $\boldsymbol{\sigma} \equiv \{\sigma_{\mu i}\}$ represents the state of the entire system, $\sigma_{\mu} = \sum_{i=1}^p \sigma_{\mu i}$ and $\boldsymbol{\sigma}_{\mu}$ are, respectively, total spin and state-vector of cluster μ and θ is an uniform external field coupled to the total spin of each cluster. The term $H_0(\boldsymbol{\sigma}_{\mu}) = -\frac{1}{2} \sum_{i \neq j} J_{ij} \sigma_{\mu i} \sigma_{\mu j}$ accounts for the intra-cluster couplings. It should be noted that, at this point, no particular choice is made for J_{ij} .

The elements of the connectivity matrix between clusters, $c_{\mu\nu}$, are chosen from a binary probability distribution

$$p(c_{\mu\nu}) = \frac{c}{N_{cl}} \delta_{c_{\mu\nu},1} + \left(1 - \frac{c}{N_{cl}}\right) \delta_{c_{\mu\nu},0} \quad (2)$$

where the constant c represents the average connectivity.

The replica method will be used to average over the quenched disorder. The disorder-averaged free energy can be written as

$$f(\beta) = - \lim_{\substack{N_{cl} \rightarrow \infty \\ n \rightarrow 0}} \frac{1}{\beta n N_{cl}} \log \langle Z^n \rangle, \quad (3)$$

where

$$Z^n = \sum_{\boldsymbol{\sigma}^1 \dots \boldsymbol{\sigma}^n} e^{-\beta \sum_{\alpha} H(\boldsymbol{\sigma}^{\alpha})} \quad (4)$$

is the replicated partition function, with $\alpha = 1 \dots n$ being the replica index. Averaging over the connectivity disorder this becomes, in the limit $c/N_{cl} \rightarrow 0$,

$$\langle Z^n \rangle = \sum_{\boldsymbol{\sigma}^1 \dots \boldsymbol{\sigma}^n} \exp \left[-\beta \sum_{\alpha \mu} H_0(\boldsymbol{\sigma}_{\mu}^{\alpha}) + \beta \theta \sum_{\alpha \mu} \sigma_{\mu}^{\alpha} + \frac{c}{2N_{cl}} \sum_{\mu \neq \nu} \left\langle e^{\frac{\beta}{\sqrt{c}} J_{\mu\nu} \sum_{\alpha} \sigma_{\mu}^{\alpha} \sigma_{\nu}^{\alpha}} - 1 \right\rangle_{J_{\mu\nu}} \right]. \quad (5)$$

Now we start to reduce to the problem of one cluster. In the following we punctuate only the main steps and refer to Appendix (A) for details. The order function in problems with finite connectivity is the probability to find the replica state vector in a given state \mathbf{s} [16, 20],

$$P(\mathbf{s}) = \frac{1}{N_{cl}} \sum_{\mu} \delta_{\mathbf{s} \boldsymbol{\sigma}_{\mu}}. \quad (6)$$

Introducing Eq. (6) in Eq. (5) the partition function becomes

$$\begin{aligned} \langle Z^n \rangle = \int \prod_{\mathbf{s}} dP(\mathbf{s}) d\hat{P}(\mathbf{s}) \exp N_{cl} \Big\{ \sum_{\mathbf{s}} \hat{P}(\mathbf{s}) P(\mathbf{s}) + \log \sum_{\mathbf{s}} \exp \Big[-\beta \sum_{\alpha} H_0(\mathbf{s}^{\alpha}) \\ + \beta \theta \sum_{\alpha} s_{\alpha} - \hat{P}(\mathbf{s}) \Big] + \frac{c}{2} \sum_{\mathbf{s} \mathbf{s}'} P(\mathbf{s}) P(\mathbf{s}') \left\langle e^{\frac{\beta J}{\sqrt{c}} \sum_{\alpha} s_{\alpha} s'_{\alpha}} - 1 \right\rangle \Big\}, \end{aligned} \quad (7)$$

where $\hat{P}(\mathbf{s})$ is an auxiliary variable and $s_{\alpha} = \sum_{i=1}^p s_{\alpha i}$. In the limit $N_{cl} \rightarrow \infty$, the integral in this equation can be solved through the saddle-point method. Eliminating $\hat{P}(\mathbf{s})$ through the saddle-point equations, the averaged per-cluster free energy

becomes

$$f(\beta) = -\lim_{n \rightarrow 0} \frac{1}{\beta n} \text{Extr} \left\{ -\frac{c}{2} \sum_{\mathbf{s}\mathbf{s}'} P(\mathbf{s})P(\mathbf{s}') \left\langle e^{\frac{\beta J}{\sqrt{c}} \sum_{\alpha} s_{\alpha} s'_{\alpha}} - 1 \right\rangle \right. \\ \left. + \log \sum_{\mathbf{s}} \exp \left[-\beta \sum_{\alpha} H_0(\mathbf{s}^{\alpha}) + \beta \theta \sum_{\alpha} s_{\alpha} + c \sum_{\mathbf{s}'} P(\mathbf{s}') \left\langle e^{\frac{\beta J}{\sqrt{c}} \sum_{\alpha} s_{\alpha} s'_{\alpha}} - 1 \right\rangle \right] \right\}. \quad (8)$$

where Extr means to take the extreme of the expression between braces relatively to $P(\mathbf{s})$. We look for solutions satisfying the replica symmetry *Ansatz* (RS), where $P(\mathbf{s})$ remains unchanged under permutation of the replica index. Since we assume that the clusters interact through their total spin, the RS *Ansatz* can be written in the form

$$P(\mathbf{s}) = \int d\mathbf{h} W(\mathbf{h}) \frac{\exp \left[-\beta \sum_{\alpha} H_0(\mathbf{s}^{\alpha}) + \beta \mathbf{h} \cdot \sum_{\alpha} \mathbf{M}(s_{\alpha}) \right]}{\left\{ \sum_{\mathbf{s}} \exp \left[-\beta H_0(\mathbf{s}) + \beta \mathbf{h} \cdot \mathbf{M}(s) \right] \right\}^n}. \quad (9)$$

Here, \mathbf{h} and $\mathbf{M}(s) \equiv (s, s^2, \dots, s^p)$ are vectors with p components, where the superscript in each components amounts to a exponent. A p -spin cluster has $p+1$ total spin states s . The component i of vector \mathbf{h} is coupled to s^i , allowing \mathbf{h} to control the population of the $p+1$ states, while the term H_0 takes account of the intra-cluster states.

All the properties of the system are accessible upon knowledge of the vector-field distribution $W(\mathbf{h})$. The RS solution reads

$$W(\mathbf{h}) = \sum_k P_k \int \prod_{l=1}^k d\mathbf{h}_l W(\mathbf{h}_l) \left\langle \prod_{i=1}^p \delta \left(h_i - \sum_l \phi_i(\mathbf{h}_l, J_l) \right) \right\rangle_{J_l}, \quad (10)$$

where h_i in the r.h.s. are components of vector \mathbf{h} in the l.h.s. and $\phi_i(\mathbf{h}_l, J_l)$, $i = 1, \dots, p$, are functions dependent on the size of the cluster. For details about the development of Eq. (10) and calculation of $\phi_i(\mathbf{h}_l, J_l)$ for $p = 3$ and $p = 4$, see the appendices. This equation can be solved recursively through a population dynamics algorithm, to be described below.

After to obtain $W(\mathbf{h})$ it is possible to calculate the observable. For example, the per cluster magnetization, the spin-glass order parameter and the occupation number are given, respectively, by

$$m = \int d\mathbf{h} W(\mathbf{h}) \langle s \rangle, \quad (11)$$

$$q = \int d\mathbf{h} W(\mathbf{h}) \langle s \rangle^2 \quad (12)$$

and

$$Q = \int d\mathbf{h} W(\mathbf{h}) \langle s^2 \rangle, \quad (13)$$

where

$$\langle s \rangle = \frac{\sum_{\mathbf{s}} s \exp [-\beta H_0(\mathbf{s}) + \beta \mathbf{h} \cdot \mathbf{M}(s)]}{\sum_{\mathbf{s}} \exp [-\beta H_0(\mathbf{s}) + \beta \mathbf{h} \cdot \mathbf{M}(s)]}, \quad (14)$$

and

$$\langle s^2 \rangle = \frac{\sum_{\mathbf{s}} s^2 \exp [-\beta H_0(\mathbf{s}) + \beta \mathbf{h} \cdot \mathbf{M}(s)]}{\sum_{\mathbf{s}} \exp [-\beta H_0(\mathbf{s}) + \beta \mathbf{h} \cdot \mathbf{M}(s)]}. \quad (15)$$

To obtain the free-energy density in the RS approach, we introduce the RS *Ansatz* in the free-energy density, Eq. (8). In the limit $n \rightarrow 0$ this results

$$\begin{aligned} f(\beta) = & \frac{c}{2\beta} \int d\mathbf{h} d\mathbf{h}' W(\mathbf{h}) W(\mathbf{h}') \quad (16) \\ & \times \frac{\left\langle \sum_{ss'} \exp \left[-\beta H_0(\mathbf{s}) + \beta \mathbf{h} \cdot \mathbf{M}(s) - \beta H_0(\mathbf{s}') + \beta \mathbf{h}' \cdot \mathbf{M}(s') + \beta \frac{J}{\sqrt{c}} ss' \right] \right\rangle_J}{\sum_{\mathbf{s}} \exp \left[-\beta H_0(\mathbf{s}) + \beta \mathbf{h} \cdot \mathbf{M}(s) \right] \sum_{\mathbf{s}'} \exp \left[-\beta H_0(\mathbf{s}') + \beta \mathbf{h}' \cdot \mathbf{M}(s') \right]} \\ & - \frac{1}{\beta} \sum_k P_k \int \prod_l d\mathbf{h}_l W(\mathbf{h}_l) \log \sum_{\mathbf{s}} \exp \left[-\beta H_0(\mathbf{s}) + \beta \theta s \right] \\ & \times \prod_l \frac{\left\langle \sum_{s_l} \exp \left[-\beta H_0(\mathbf{s}_l) + \beta \mathbf{h}_l \cdot \mathbf{M}(s_l) + \beta \frac{J_l}{\sqrt{c}} ss_l \right] \right\rangle_{J_l}}{\sum_{\mathbf{s}} \exp \left[-\beta H_0(\mathbf{s}) + \beta \mathbf{h}_l \cdot \mathbf{M}(s) \right]}. \end{aligned}$$

Linear Magnetic Susceptibility

The linear magnetic susceptibility $\chi = (\partial m / \partial \theta)_{\theta \rightarrow 0} = -(\partial^2 f / \partial \theta^2)_{\theta \rightarrow 0}$ plays a central role in characterizing geometrical frustration [2]. From Eq. (8) we have

$$\frac{\partial^2 f}{\partial \theta^2} = -\frac{\beta}{n} \sum_{\mathbf{s}} P(\mathbf{s}) \left(\sum_{\alpha} s_{\alpha} \right)^2 + \frac{\beta}{n} \left(\sum_{\mathbf{s}} P(\mathbf{s}) \sum_{\alpha} s_{\alpha} \right)^2. \quad (17)$$

In the limit $n \rightarrow 0$ the second term vanishes and the first can be written in terms of q and Q , and then

$$\chi = \beta(Q - q). \quad (18)$$

Stability of RS solution

The stability of the RS solution was determined by using the two replica method [18]. It consists in solving the saddle-point equations for two independent systems, only coupled through the disorder realization. The Hamiltonian for the double system reads

$$\begin{aligned} H(\boldsymbol{\sigma}, \boldsymbol{\tau}) = & -\frac{1}{2\sqrt{c}} \sum_{\mu \neq \nu} c_{\mu\nu} J_{\mu\nu} \sigma_{\mu} \sigma_{\nu} - \frac{1}{2\sqrt{c}} \sum_{\mu \neq \nu} c_{\mu\nu} J_{\mu\nu} \tau_{\mu} \tau_{\nu} \\ & - \theta \sum_{\mu} \sigma_{\mu} - \theta \sum_{\mu} \tau_{\mu} + \sum_{\mu} H_0(\sigma_{\mu}) + \sum_{\mu} H_0(\tau_{\mu}) \end{aligned} \quad (19)$$

The self-consistent equation for the two-replica vector field distribution is

$$\begin{aligned} W(\mathbf{h}, \mathbf{h}') = & \sum_k P_k \int \prod_{l=1}^k d\mathbf{h}_l d\mathbf{h}'_l W(\mathbf{h}_l) W(\mathbf{h}'_l) \\ & \times \left\langle \prod_{i=1}^p \left[\delta \left(h_i - \sum_l \phi_i(\mathbf{h}_l, J_l) \right) \delta \left(h'_i - \sum_l \phi_i(\mathbf{h}'_l, J_l) \right) \right] \right\rangle_{J_l}, \end{aligned} \quad (20)$$

which is diagonal, i.e.,

$$W(\mathbf{h}, \mathbf{h}') = W(\mathbf{h}) \delta(\mathbf{h} - \mathbf{h}') \quad (21)$$

if RS solution is stable and non-diagonal otherwise. The AT line is found by calculating the overlap between two replicas,

$$q' = \int d\mathbf{h} d\mathbf{h}' W(\mathbf{h}, \mathbf{h}') \langle s \rangle(\mathbf{h}) \langle s \rangle(\mathbf{h}'). \quad (22)$$

From Eqs. (12) and (21), $q' = q$ if RS is stable, and the appearing of a bifurcation signals the AT line.

III. RESULTS AND DISCUSSIONS

Two types of cluster geometry are considered: the equilateral triangle, $p = 3$ and the regular tetrahedron, $p = 4$, as shown in Figs. 1(a) and 1(b), respectively. For simplicity, the inner couplings J_0/J are uniform, although the theoretical framework allows to consider non-uniform couplings as well. Our analysis focuses in the interplay between the two geometries, the intra-cluster couplings J_0/J and how it is affected by the connectivity c . Due to frustration effects, the most interesting is the region $J_0/J < 0$. The standard deviation of the Gaussian distributed inter-cluster couplings J is adopted as the energy scale.

The relevant observable are obtained upon the solution of the self consistent saddle point equation (10) through a population dynamics algorithm [19, 21], as follows. Initially, a population of size \mathcal{N} of p -dimensional vector-fields is created with a certain starting guess. In each iteration, a number k is chosen from a Poisson distribution of mean c ; k vector fields \mathbf{h}_l and couplings J_l , $l = 1 \dots k$, are randomly chosen; the l -summation in each Dirac's δ -function in Eq. (10) is calculated. Finally, another field is randomly chosen from the population and to each of its components is assigned the corresponding l -summation. This procedure is repeated till the population of vector-fields converges.

To visualize a vector-field distribution, it is convenient to use marginal distribu-

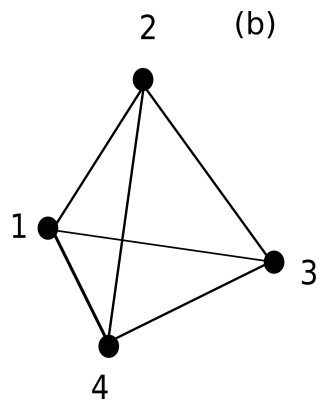
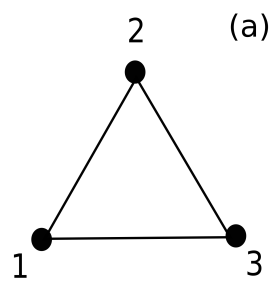


FIG. 1. (a) Triangular and (b) tetrahedral clusters.

tions,

$$w(h_i) = \int \prod_{j \neq i} dh_j W(\mathbf{h}), \quad (23)$$

where j runs over all fields but i . Examples of the marginal distributions for triangular clusters are drawn in Fig. 2, where the system is in a CSG phase with $q > 0$ and $Q > 0$. Whenever $q > 0$, $q' \neq q$, so the RS solution is unstable into the CSG phase and, as a consequence, the AT line coincides with the CSG phase boundary.

Next, to provide a better discussion, we present the results for each cluster geometry in two separated subsections.

A. Triangular clusters

The macroscopic state is determined by calculating the order parameters q and Q through Eqs. (12) and (13), respectively, for a set of chosen values of c and a proper range of J_0/J . To show how this unveils, Fig. 3 shows the phase diagram T/J versus J_0/J for several values of c . There, two types of magnetic states are observed. At high temperature, a paramagnetic (PM) phase with $Q > 0$ and $q = 0$ is found. Then, decreasing the temperature, there is a continuous transition to a CSG phase, with $Q > 0$ and $q > 0$, at the freezing temperature T_f/J . Moreover, as it will be discussed below, in a region with strong AF couplings, and therefore strong GF, there appears a crossover from the PM phase to a classical SL state at the temperature T^*/J , at a temperature above the onset of the CSG. In particular, for $J_0/J < -3.0$, T_f/J becomes independent of J_0/J , while T^*/J becomes linearly dependent on it. Concerning the role of c , the phase diagram can be divided in three regions, depending on J_0/J . In the first region, with $J_0/J \gtrsim -1.5$, T_f/J increases as c increases. There is a second region, for $-2.5 \lesssim J_0/J \lesssim -1.5$, T_f/J decreases as c increases. Finally, for $J_0/J \lesssim -2.5$, T_f/J returns to increase with increasing c . It is

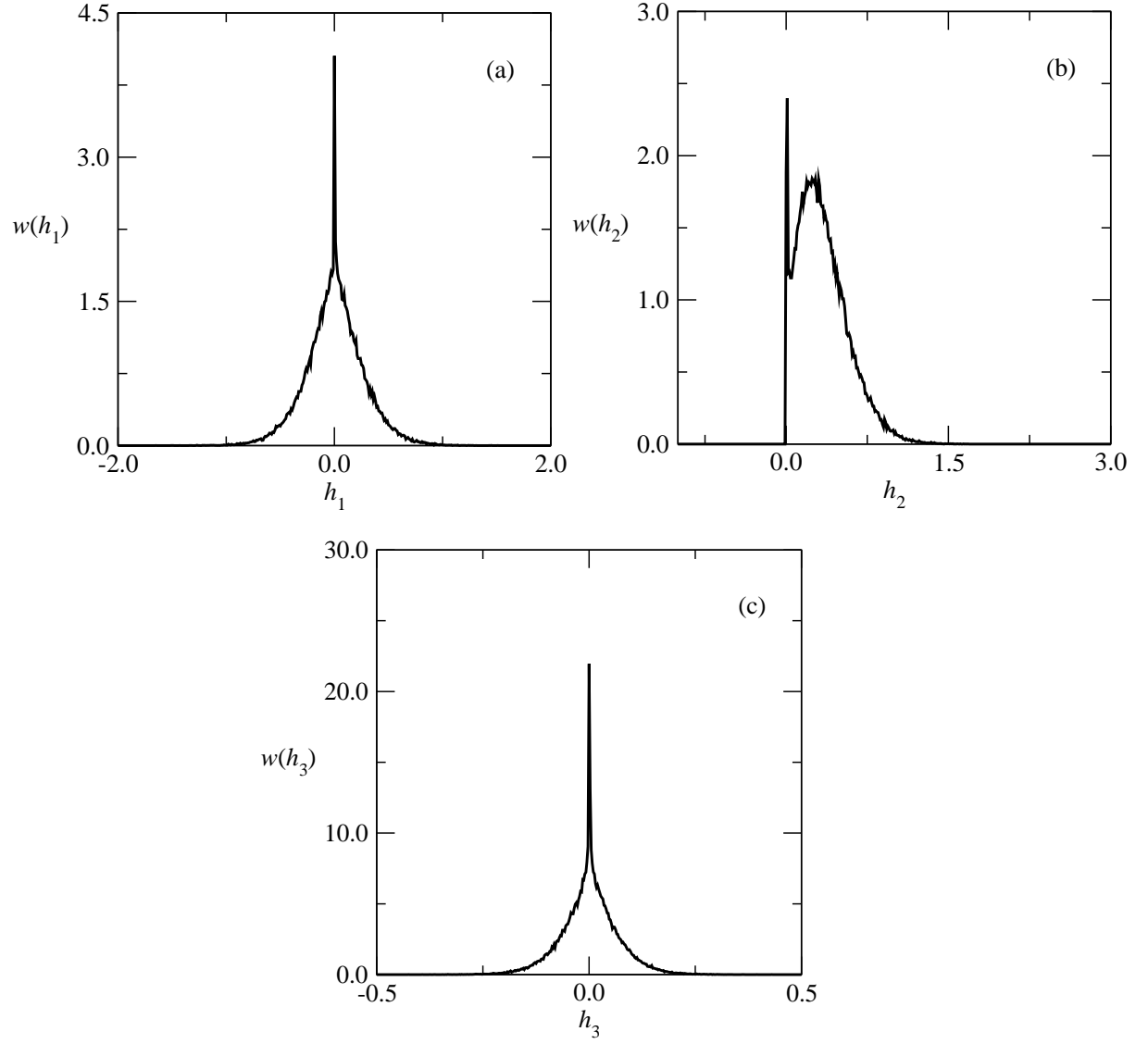


FIG. 2. Marginal distributions for each component of a triangular cluster, for $T/J = 0.1$, $c = 4$ and $J_0/J = -5.0$, where there are strong frustration effects (see discussion below). $\mathcal{N} = 10^5$ is the size of the population of fields. (a) Marginal along the h_1 field, (b) marginal along the h_2 field and (c) marginal along the h_3 field.

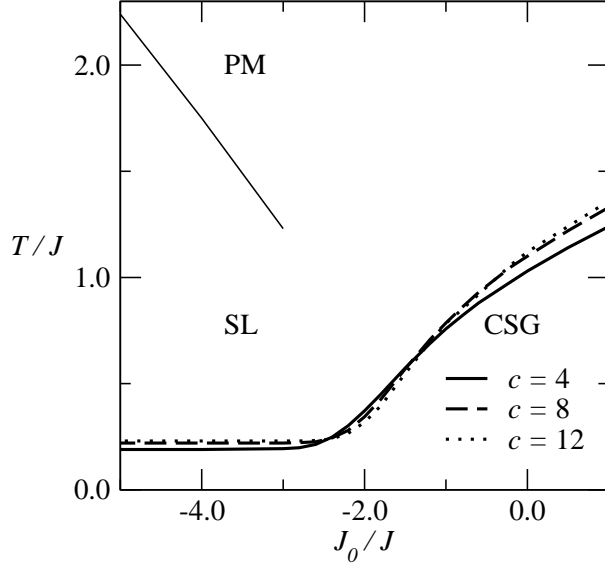


FIG. 3. T/J versus J_0/J phase diagrams in clusters of equilateral triangles. The thin line represents the SL to PM crossover temperature T^*/J .

worth to mention that in the range that was investigated, T_f/J is weakly dependent on c , and it converges to the infinite connectivity behavior beyond $c \gtrsim 12$.

To proceed our analysis, the entropy per cluster $s = -\partial f / \partial T$ and the magnetic specific heat $C_m = -T \partial^2 f / \partial T^2$ were calculated. In Fig. 4(a) s and C_m are drawn for two representative values of J_0/J . The entropy plateau prior the CSG phase transition leads to a C_m showing a two-maxima structure. There is a low temperature maximum that is relative to the loss in degrees of freedom close to the CSG transition. As the temperature continues to increase, there is a second, less pronounced maximum in C_m , at T^*/J . Its position varies linearly with J_0/J , as shown by the thin line in the phase diagram in Fig. 3. Strictly speaking, there is no thermodynamic transition at T^*/J , since no order parameter are going to zero there. In fact, the interval $T_f/J < T/J < T^*/J$ has always $q = 0$. Nevertheless, the high temperature maximum suggests that in between the two maxima, a different paramagnetic

order settles in, where internal to the clusters degrees of freedom dominate. This region corresponds to the classical SL displayed in Fig 3. Thus, we amount T^*/J as temperature crossover between the PM phase and the classical SL [22].

To investigate the connectivity dependence on T^*/J , plots of C_m vs. T/J for two representative values of c are shown in Fig. 4(b). For $c = 8$, the first C_m maximum gets higher and is horizontally dislocated. This is consistent with a similar effect on T_f/J . Moreover, a further decrease on c makes this maximum eventually disappear at the percolation limit $c = 1$. The second maximum is marginally modified by changing c . This means that T^*/J does not depend on the random network connectivity.

The interplay between of c and J_0/J is also investigated regarding the level of GF given by the parameter $f_p = |\Theta_{CW}|/T_f$ [2], where Θ_{CW} is the Curie-Weiss temperature. We show in Fig. 5(a), the inverse of susceptibility χ^{-1} displaying a cusp at T_f/J , which is characteristic of a spin glass-like transition. χ^{-1} is plotted for c ranging from 2 to 12. For $T/J \gg T_f/J$, the behaviour of χ^{-1} does not change with an increase in c . However, as can be noted in Fig. 5(b), Θ_{CW}/J is highly influenced by changing J_0/J . Θ_{CW}/J was estimated through the Curie-Weiss law $\chi(T) = C/(T - \Theta_{CW})$, from the linear region of the χ^{-1} vs. T/J curves. For $J_0/J = -3.0$, the obtained value is $\Theta_{CW}/J \approx -1.84$ for all c . For $c = 4$, we obtain $f_p \approx 9.46$, thus indicating a moderate frustrated scenario. As can be observed, Θ_{CW}/J strongly depends on J_0/J , but f_p is also a function of T_f/J which, by its turn, is influenced by c .

To visualize how the interplay between c and J_0/J reflects on the level of frustration, curves of f_p vs c^{-1} for three values of J_0/J , are presented in Fig. 6. This allows to identify important differences in the behavior of f_p , as follows. For $J_0/J = -2.0$, f_p is relatively weakly affected by the variation of c , but it is important to remark that there is a minimum of frustration at $c \approx 3$. This interesting point deserves further investigation to be explained. In strong contrast, for $J_0/J = -5.0$, f_p presents

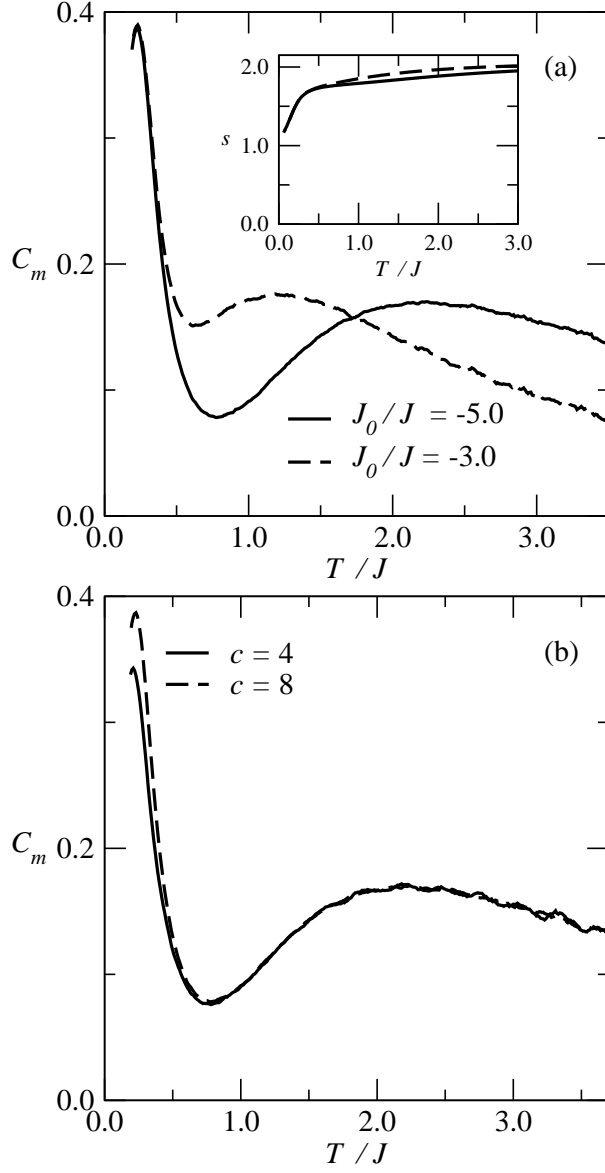


FIG. 4. (a) Specific heat C_m vs. T/J for intra-cluster couplings $J_0/J = -5.0$ and $J_0/J = -3.0$, for $c = 4$. The inset shows the corresponding entropy. (b) Specific heat C_m versus T/J for $c = 4$ and $c = 8$, for $J_0/J = -3.0$.

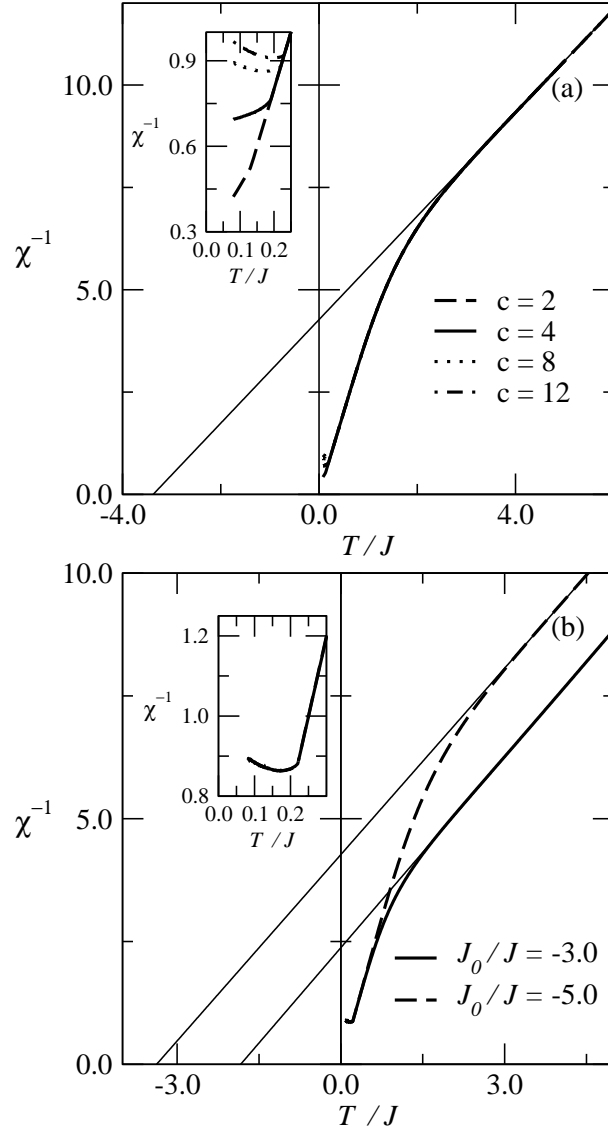


FIG. 5. (a) Inverse susceptibility χ^{-1} versus T/J profiles for fixed intra-cluster couplings $J_0/J = -5.0$ and connectivity values $c = 2, c = 4, c = 8$ and $c = 12$. The inset shows the cusps in detail. (b) Inverse susceptibility χ^{-1} vs. T/J profiles for fixed $c = 8$ and two values of the intra-cluster couplings: $J_0/J = -3.0$ and $J_0/J = -5.0$. The inset shows the cusps in detail. The thin straight lines represent the fit of the Curie-Weiss law to the linear region of χ^{-1} .

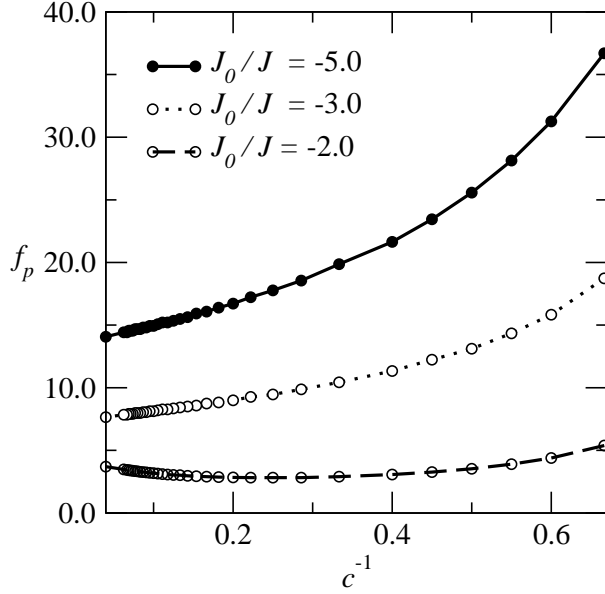


FIG. 6. Frustration parameter f_p vs. c^{-1} .

a fast growing as c decreases. This behaviour (as for $J_0/J = -3.0$), is coherent with the development of a SL region obtained in the phase diagram of Fig. 3. We could not go further beyond $c^{-1} \approx 0.7$ in Fig. 6 because the freezing temperature T_f/J approaches zero as $c \rightarrow 1$, causing numerical instability. Anyway, since Θ_{CW}/J is nearly c -independent, the f_p parameter should diverge in this limit.

B. Tetrahedral clusters

There are two major differences relative to the triangular clusters. Firstly, the cluster is not prone to geometrical frustration. Secondly, the cluster can be fully compensated, i.e., there exist states where the total spin of the cluster Q is zero. For instance, for $J_0/J \ll 0$ the full compensation is favoured, as will be discussed below. Another consequence is that, contrary to triangular clusters, discontinuous

transitions do appear for sufficiently large c . We refer to Figure 7 as an example of the curves for Q and q versus J_0/J in the vicinity of a first order CSG-PM transition, for $c = 8$. The free energy f , that allows to localise the first order transition, is also shown.

The general behaviour of tetrahedral clusters can be resumed in the phase diagram of Fig. 8. The most interesting regime is $J_0/J < 0$. For $J_0/J > 0$ the clusters become frozen at its maximum Q value. As stated above, for $J_0/J \ll 0$, the fundamental state is fully compensate. This means that the total cluster spin assumes the state $s = 0$, favouring a non-magnetic state, with $q = 0 = Q$. As J_0/J become less negative, the ground state becomes the CSG phase. This occurs at $J_0/J \geq -1.95$ and is due to the increase in relevance of the long range random interactions.

As shown in Figure 8, there is a remarkable influence of the connectivity between clusters on the phase diagrams. For low connectivity, as $c = 4$, the PM \rightarrow CSG phase transition is always continuous. Contrary, already for $c = 8$, a more complex picture appears, with a low-temperature discontinuous transition, a high-temperature continuous transition and a tricritical point between them. For $c = 8$ and $c = 12$, the tricritical point are located at $T_c/J = 0.18$ and $T_c/J = 0.24$, respectively.

Associated to the discontinuous PM \rightarrow CSG transitions, Fig. 8 shows a reentrant region. At the transition, the CSG phase co-exists with the PM phase with small Q [23]. In the reentrant region the system passes from PM to CSG and then to PM. This re-entrance is similar to the unusual inverse freezing phase transition observed in non-Ising classical models [24, 25], and is related to the full compensation of the total cluster spin at large negative J_0/J . At low temperature, the fully compensated, non-magnetic cluster state is favoured. This becomes no longer true when thermal fluctuations increase, and the long-range, disordered interaction, acts to stabilize a CSG phase. Since this is a collective effect, it depends on the connectivity. Although the re-entrance, the principle of monotonic increase of entropy with temperature is

not violated, since the small Q phase has lower entropy than the CSG one that is at higher temperature.

IV. CONCLUDING REMARKS

In this paper, we developed a novel theoretical framework to take into account geometric frustration effects within the cluster magnetism with disorder in a sparse random network, where the connectivity between clusters is a controllable parameter. We have used a triangle and a tetrahedral for choices of the inner cluster structure. The intra-cluster interaction for both cases is anti-ferromagnetic (AF).

Our results show that, for the triangular cluster geometry, the Cluster Spin Glass ground state appears even for very small disorder. Most importantly, such result does not depend on the cluster network connectivity. Furthermore, geometric frustration effects lead to a classical spin-liquid region which is dependent on the strength of intra-cluster AF interaction J_0/J but is very weakly dependent of the connectivity. On the other hand, variations in the connectivity strongly affects the level of frustration $f_p = -\Theta_{CW}/T_f$ for larger value of J_0/J . This behaviour is particularly intense for larger values of J_0/J . Thus, the increase of f_p is consistent with the development of the SL region.

In the case of the tetragonal cluster geometry there appears, at low temperature, the unusual phase transition known as inverse freezing [24], that is similar to those results already obtained for the fully connect network of clusters (see, for instance, Ref. [23]). Our results show that, in the case of a low connectivity, the inverse freezing disappears, which indicates that this unusual phase transition is connectivity dependent.

To summarize, the relationship between cluster magnetism, disorder and geometric frustration was studied. For this purpose, we introduced a novel methodology in

which the cluster network connectivity is a controllable parameter of the theory. We investigate two particular types of cluster geometry. However, we do believe that the method can be extended to other kinds of cluster geometry, as for instance, the kagome one. We are currently investigating this point. Furthermore, although in this paper the intra-cluster couplings were uniform, the theory can be applied to the non-uniform case.

ACKNOWLEDGMENTS

The authors would like to thank Prof. Mateus Schmidt for discussions. The present study was supported by the Brazilian agencies Conselho Nacional de Desenvolvimento Científico e Tecnológico (CNPq), Coordenação de Aperfeiçoamento de Pessoal de Nível Superior (CAPES) and Fundação de Amparo à pesquisa do Estado do RS (FAPERGS).

Appendix A: derivation of the saddle-point equations

In order to reduce to the problem of one cluster, the first step is to withdraw the total spin of the clusters from the inner exponential in Eq. 5, using the identity

$$1 = \sum_{\mathbf{s}} \prod_{\alpha=1}^n \prod_{i=1}^p \delta_{s_i^\alpha \sigma_{\mu i}^\alpha} = \sum_{\mathbf{s}} \delta_{\mathbf{s} \boldsymbol{\sigma}_\mu}, \quad (\text{A1})$$

where $\delta_{s\sigma}$ is the Kronecker's delta and $\mathbf{s} \equiv \{s_i^\alpha\}$ is an auxiliary spin vector.

The replicated partition function becomes

$$\begin{aligned} \langle Z^n \rangle = \sum_{\boldsymbol{\sigma}^1 \dots \boldsymbol{\sigma}^n} \exp \Big[& -\beta \sum_{\alpha\mu} H_0(\boldsymbol{\sigma}_\mu^\alpha) + \beta\theta \sum_{\alpha\mu} \sigma_\mu^\alpha \\ & + \frac{c}{2N_{cl}} \sum_{\mu \neq \nu} \sum_{\mathbf{s}\mathbf{s}'} \delta_{\mathbf{s}\boldsymbol{\sigma}_\mu} \delta_{\mathbf{s}'\boldsymbol{\sigma}_\nu} \left\langle e^{\frac{\beta J}{\sqrt{c}} \sum_{\alpha} s_{\alpha} s'_{\alpha}} - 1 \right\rangle_J \Big], \end{aligned} \quad (\text{A2})$$

where $s_\alpha = \sum_{i=1}^p s_i^\alpha$.

The order function, Eq. (6), is introduced in Eq. (5) through a Dirac's delta function and then, using the integral representation for the Dirac's delta function, the replicated partition function becomes

$$\begin{aligned} \langle Z^n \rangle = & \sum_{\sigma^1 \dots \sigma^n} \int \prod_{\mathbf{s}} dP(\mathbf{s}) d\hat{P}(\mathbf{s}) \exp \left\{ -\beta \sum_{\alpha\mu} H_0(\sigma_\mu^\alpha) + \beta\theta \sum_{\alpha\mu} \sigma_\mu^\alpha + \sum_{\mathbf{s}} \hat{P}(\mathbf{s}) P(\mathbf{s}) \right. \\ & \left. - \frac{1}{N_{cl}} \sum_{\mathbf{s}} \hat{P}(\mathbf{s}) \sum_{\mu} \delta_{\mathbf{s}\sigma_\mu} + \frac{cN_{cl}}{2} \sum_{\mathbf{s}\mathbf{s}'} P(\mathbf{s}) P(\mathbf{s}') \left\langle e^{\frac{\beta J}{\sqrt{c}} \sum_{\alpha} s_{\alpha} s'_{\alpha}} - 1 \right\rangle_J \right\}. \end{aligned} \quad (\text{A3})$$

The summation over the spin variables $\sigma_\mu^\alpha = (\sigma_{\mu 1}^\alpha \dots \sigma_{\mu p}^\alpha)$ concerns the factor

$$\% = \sum_{\sigma^1 \dots \sigma^n} \exp \left[-\beta \sum_{\alpha\mu} H_0(\sigma_\mu^\alpha) + \beta\theta \sum_{\alpha\mu} \sigma_\mu^\alpha - \frac{1}{N_{cl}} \sum_{\mathbf{s}} \hat{P}(\mathbf{s}) \sum_{\mu} \delta_{\mathbf{s}\sigma_\mu} \right]. \quad (\text{A4})$$

Summing over \mathbf{s} in the second term of the exponential and rearranging terms, this becomes

$$\% = \prod_{\mu} \sum_{\sigma_\mu} \exp \left[-\beta \sum_{\alpha} H_0(\sigma_\mu^\alpha) + \beta\theta \sum_{\alpha} \sigma_\mu^\alpha - \frac{1}{N_{cl}} \hat{P}(\sigma_\mu) \right]. \quad (\text{A5})$$

Since the clusters are decoupled, this reduces to the problem of one cluster, and can be expressed as

$$\% = \exp N_{cl} \log \sum_{\mathbf{s}} \exp \left[-\beta \sum_{\alpha} H_0(\mathbf{s}^\alpha) + \beta\theta \sum_{\alpha} s_{\alpha} - \frac{1}{N_{cl}} \hat{P}(\mathbf{s}) \right]. \quad (\text{A6})$$

Changing variables $\hat{P} \rightarrow N_{cl} \hat{P}$, we obtain Eq. (7).

Introducing Eq. (7) in Eq. (3), the averaged per-cluster free energy reads

$$\begin{aligned} f(\beta) = & -\lim_{n \rightarrow 0} \frac{1}{\beta n} \text{Extr} \left\{ \sum_{\mathbf{s}} \hat{P}(\mathbf{s}) P(\mathbf{s}) + \log \sum_{\mathbf{s}} \exp \left[-\beta \sum_{\alpha} H_0(\mathbf{s}^\alpha) + \beta\theta \sum_{\alpha} s_{\alpha} - \hat{P}(\mathbf{s}) \right] \right. \\ & \left. + \frac{c}{2} \sum_{\mathbf{s}\mathbf{s}'} P(\mathbf{s}) P(\mathbf{s}') \left\langle e^{\frac{\beta J}{\sqrt{c}} \sum_{\alpha} s_{\alpha} s'_{\alpha}} - 1 \right\rangle \right\}, \end{aligned} \quad (\text{A7})$$

where Extr means to take the extreme of the expression between braces relatively to variables $\hat{P}(\mathbf{s})$ and $P(\mathbf{s})$. This is imposed by the saddle-point equations

$$\frac{\partial f(\beta)}{\partial \hat{P}(\mathbf{s})} = 0 = \frac{\partial f(\beta)}{\partial P(\mathbf{s})}, \quad (\text{A8})$$

which are written as

$$P(\mathbf{s}) = \frac{\exp \left[-\beta \sum_{\alpha} H_0(\mathbf{s}^{\alpha}) + \beta \theta \sum_{\alpha} s_{\alpha} - \hat{P}(\mathbf{s}) \right]}{\sum_{\mathbf{s}'} \exp \left[-\beta \sum_{\alpha} H_0(\mathbf{s}'^{\alpha}) + \beta \theta \sum_{\alpha} s'_{\alpha} - \hat{P}(\mathbf{s}') \right]} \quad (\text{A9})$$

and

$$\hat{P}(\mathbf{s}) = -c \sum_{\mathbf{s}'} P(\mathbf{s}') \left\langle e^{\frac{\beta J}{\sqrt{c}} \sum_{\alpha} s_{\alpha} s'_{\alpha}} - 1 \right\rangle. \quad (\text{A10})$$

Eliminating $\hat{P}(\mathbf{s})$ in Eq. (A9), we obtain a self-consistent equation for $P(\mathbf{s})$:

$$P(\mathbf{s}) = \frac{\exp \left[-\beta \sum_{\alpha} H_0(\mathbf{s}^{\alpha}) + \beta \theta \sum_{\alpha} s_{\alpha} + c \sum_{\mathbf{s}'} P(\mathbf{s}') \left\langle e^{\frac{\beta J}{\sqrt{c}} \sum_{\alpha} s_{\alpha} s'_{\alpha}} - 1 \right\rangle \right]}{\sum_{\mathbf{s}'} \exp \left[-\beta \sum_{\alpha} H_0(\mathbf{s}'^{\alpha}) + \beta \theta \sum_{\alpha} s'_{\alpha} + c \sum_{\mathbf{s}''} P(\mathbf{s}'') \left\langle e^{\frac{\beta J}{\sqrt{c}} \sum_{\alpha} s'_{\alpha} s''_{\alpha}} - 1 \right\rangle \right]}. \quad (\text{A11})$$

Introducing Eqs. (A10) and (A11) in Eq. (A7) we obtain the per cluster free-energy, Eq. (8).

To obtain the vector local-field distribution, Eq. (10), we introduce the RS *Ansatz*, Eq. (9), in the saddle-point equation, Eq. (A11). Since $P(\mathbf{s})$ is a probability, the denominator on the r.h.s. of Eq. (A11) is equal to 1. Expanding the exponential on the numerator, we have

$$P(\mathbf{s}) = \exp \left[-\beta \sum_{\alpha} H_0(\mathbf{s}^{\alpha}) + \beta \theta \sum_{\alpha} s_{\alpha} \right] \sum_k P_k \prod_{l=1}^k \sum_{\mathbf{s}_l} \int d\mathbf{h}_l W(\mathbf{h}_l) \quad (\text{A12})$$

$$\times \frac{\left\langle \exp \left[-\beta \sum_{\alpha} H_0(\mathbf{s}_l^{\alpha}) + \beta \mathbf{h}_l \cdot \sum_{\alpha} \mathbf{M}(s_{\alpha l}) + \beta \frac{J_l}{\sqrt{c}} \sum_{\alpha} s_{\alpha} s_{\alpha l} \right] \right\rangle_{J_l}}{\left\{ \sum_{\mathbf{s}} \exp \left[-\beta H_0(\mathbf{s}) + \beta \mathbf{h}_l \cdot \mathbf{M}(\mathbf{s}) \right] \right\}^n},$$

where $P_k = \sum_k e^{-c} c^k / k!$ is a Poissonian weight. Rearranging terms, this can be rewritten as

$$P(\mathbf{s}) = \exp \left[-\beta \sum_{\alpha} H_0(\mathbf{s}^{\alpha}) + \beta \theta \sum_{\alpha} s_{\alpha} \right] \sum_k P_k \int \prod_{l=1}^k d\mathbf{h}_l W(\mathbf{h}_l) \quad (\text{A13})$$

$$\times \frac{\left\langle \exp \sum_{\alpha} \sum_s \delta_{ss_{\alpha}} \log \chi_s(\mathbf{h}_l, J_l) \right\rangle_{J_l}}{\chi_0^n(\mathbf{h}_l, 0)},$$

where

$$\chi_s(\mathbf{h}, J) = \sum_{\mathbf{s}'} \exp \left[-\beta H_0(\mathbf{s}') + \beta \mathbf{h} \cdot \mathbf{M}(s') + \beta \frac{J}{\sqrt{c}} s s' \right] \quad (\text{A14})$$

and the Kroenecker's delta was introduced to factorize the replica index α . If s and s_{α} are $p+1$ -state spin variables, $\delta_{ss_{\alpha}}$ is a symmetric polynomial in powers of s and s_{α} . Introducing the corresponding Kroenecker's delta and summing over the spin variables \mathbf{s} , Eq. (A13) can be written in the form

$$P(\mathbf{s}) = \sum_k P_k \int \prod_{l=1}^k d\mathbf{h}_l W(\mathbf{h}_l) \quad (\text{A15})$$

$$\times \frac{\left\langle \exp \left[-\beta \sum_{\alpha} H_0(\mathbf{s}^{\alpha}) + \beta n \sum_l \phi_0(\mathbf{h}_l, J_l) + \beta \sum_l \boldsymbol{\phi}(\mathbf{h}_l, J_l) \cdot \sum_{\alpha} \mathbf{M}(s_{\alpha}) \right] \right\rangle_{J_l}}{\chi_0^n(\mathbf{h}_l, 0)}.$$

Here, $\boldsymbol{\phi}(\mathbf{h}, J)$ denotes a p -component vector whose components are the functions $\phi_i(\mathbf{h}, J)$. The zeroth component need not to be calculated, since at the end we will take the limit $n \rightarrow 0$. A detailed calculation, as well as the derivation of the vector $\boldsymbol{\phi}(\mathbf{h}, J)$ for triangular and tetragonal lattices will be shown in Appendices B and C, respectively. Introducing the RS “Ansatz” in the l.h.s. and considering that the

denominator in the r.h.s. goes to 1, Eq. (A15) becomes

$$\begin{aligned}
& \int d\mathbf{h} W(\mathbf{h}) \exp \left[-\beta \sum_{\alpha} H_0(\mathbf{s}^{\alpha}) + \beta \mathbf{h} \cdot \sum_{\alpha} \mathbf{M}(s_{\alpha}) \right] \\
&= \sum_k P_k \int \prod_{l=1}^k d\mathbf{h}_l W(\mathbf{h}_l) \left\langle \exp \left[-\beta \sum_{\alpha} H_0(\mathbf{s}^{\alpha}) \right. \right. \\
&\quad \left. \left. + \beta \sum_l \phi(\mathbf{h}_l, J_l) \cdot \sum_{\alpha} \mathbf{M}(s_{\alpha}) \right] \right\rangle_{J_l}.
\end{aligned} \tag{A16}$$

Introducing a Dirac's delta function for each component of the field vector \mathbf{h} in the r.h.s. of Eq. (A16) we have

$$\begin{aligned}
& \int d\mathbf{h} W(\mathbf{h}) \exp \left[-\beta \sum_{\alpha} H_0(\mathbf{s}^{\alpha}) + \beta \mathbf{h} \cdot \sum_{\alpha} \mathbf{M}(s_{\alpha}) \right] \\
&= \int d\mathbf{h} \sum_k P_k \int \prod_{l=1}^k d\mathbf{h}_l W(\mathbf{h}_l) \left\langle \prod_{i=1}^p \delta \left(h_i - \sum_l \phi_i(\mathbf{h}_l, J_l) \right) \right\rangle_{J_l} \\
&\quad \times \exp \left[-\beta \sum_{\alpha} H_0(\mathbf{s}^{\alpha}) + \beta \mathbf{h} \cdot \sum_{\alpha} \mathbf{M}(s_{\alpha}) \right].
\end{aligned} \tag{A17}$$

Comparing both sides of Eq. (A17) we obtain Eq. (10).

Appendix B: 3-spins clusters

The cluster spin assumes four states: $-3/2, -1/2, 1/2, 3/2$. The four-state Kronecker's delta reads

$$\delta_{ss_{\alpha}} = \frac{41}{64} - \frac{5}{16}(s^2 + s_{\alpha}^2) + \frac{365}{144}ss_{\alpha} - \frac{41}{36}(s^3 s_{\alpha} + ss_{\alpha}^3) + \frac{1}{4}s^2 s_{\alpha}^2 + \frac{5}{9}s^3 s_{\alpha}^3. \tag{B1}$$

Introducing Eq. (B1) in Eq. (A13), summing over s and rearranging terms we obtain Eq. (A15), with

$$\beta \phi_1(\mathbf{h}, J) = \frac{\theta}{k} + \frac{27}{24} \log \frac{\chi_{\frac{1}{2}}(\mathbf{h}, J)}{\chi_{-\frac{1}{2}}(\mathbf{h}, J)} - \frac{1}{24} \log \frac{\chi_{\frac{3}{2}}(\mathbf{h}, J)}{\chi_{-\frac{3}{2}}(\mathbf{h}, J)}, \tag{B2}$$

$$\beta\phi_2(\mathbf{h}, J) = -\frac{1}{4} \log \chi_{\frac{1}{2}}(\mathbf{h}, J) \chi_{-\frac{1}{2}}(\mathbf{h}, J) + \frac{1}{4} \log \chi_{\frac{3}{2}}(\mathbf{h}, J) \chi_{-\frac{3}{2}}(\mathbf{h}, J), \quad (\text{B3})$$

and

$$\beta\phi_3(\mathbf{h}, J) = -\frac{1}{2} \log \frac{\chi_{\frac{1}{2}}(\mathbf{h}, J)}{\chi_{-\frac{1}{2}}(\mathbf{h}, J)} + \frac{1}{6} \log \frac{\chi_{\frac{3}{2}}(\mathbf{h}, J)}{\chi_{-\frac{3}{2}}(\mathbf{h}, J)}. \quad (\text{B4})$$

Appendix C: 4-spins clusters

The cluster spin assumes five states: $-2, -1, 0, 1, 2$. The five-state Kroenecker's delta reads

$$\begin{aligned} \delta_{ss_\alpha} = 1 - \frac{5}{4}(s^2 + s_\alpha^2) + \frac{65}{72}ss_\alpha + \frac{1}{4}(s^4 + s_\alpha^4) - \frac{17}{72}(s^3s_\alpha + ss_\alpha^3) \\ + \frac{707}{288}s^2s_\alpha^2 - \frac{155}{288}(s^4s_\alpha^2 + s^2s_\alpha^4) + \frac{5}{72}s^3s_\alpha^3 + \frac{35}{288}s^4s_\alpha^4. \end{aligned} \quad (\text{C1})$$

Introducing Eq. (C1) in Eq. (A13), summing over s and rearranging terms we obtain Eq. (A15), with

$$\beta\phi_1(\mathbf{h}, J) = \frac{\theta}{k} - \frac{1}{12} \log \frac{\chi_{+2}(\mathbf{h}, J)}{\chi_{-2}(\mathbf{h}, J)} + \frac{2}{3} \log \frac{\chi_{+1}(\mathbf{h}, J)}{\chi_{-1}(\mathbf{h}, J)}, \quad (\text{C2})$$

$$\beta\phi_2(\mathbf{h}, J) = -\frac{1}{24} \log \chi_{+2}(\mathbf{h}, J) \chi_{-2}(\mathbf{h}, J) + \frac{2}{3} \log \chi_{+1}(\mathbf{h}, J) \chi_{-1}(\mathbf{h}, J) - \frac{5}{4} \log \chi_0(\mathbf{h}, J), \quad (\text{C3})$$

$$\beta\phi_3(\mathbf{h}, J) = \frac{1}{12} \log \frac{\chi_{+2}(\mathbf{h}, J)}{\chi_{-2}(\mathbf{h}, J)} - \frac{1}{6} \log \frac{\chi_{+1}(\mathbf{h}, J)}{\chi_{-1}(\mathbf{h}, J)}, \quad (\text{C4})$$

$$\beta\phi_4(\mathbf{h}, J) = \frac{1}{24} \log \chi_{+2}(\mathbf{h}, J) \chi_{-2}(\mathbf{h}, J) - \frac{1}{6} \log \chi_{+1}(\mathbf{h}, J) \chi_{-1}(\mathbf{h}, J) + \frac{1}{4} \log \chi_0(\mathbf{h}, J). \quad (\text{C5})$$

[1] A. Furrer and O. Waldmann, Rev. Mod. Phys. **85**, 367 (2013).

- [2] A. P. Ramirez, Annual Review of Materials Science **24**, 453 (1994).
- [3] C. Lacroix, P. Mendels, and F. Mila, *Introduction to Frustrated Magnetism: Materials, Experiments, Theory* (Springer, 2011).
- [4] L. Balents, Nature **464**, 199 (2010).
- [5] S. Pakhira, C. Mazundar, R. Ranganathan, and M. Avdeev, Scientific Reports **7**, 1 (2017).
- [6] M. E. Zhitomirsky, Phys. Rev. B **67**, 104421 (2003).
- [7] C. M. Soukoulis, Phys. Rev. B **18**, 3757 (1978).
- [8] C. M. Soukoulis and K. Levin, Phys. Rev. B **18**, 1439 (1978).
- [9] S. Bedanta and W. Kleemann, Journal of Physics D: Applied Physics **42**, 013001 (2008).
- [10] M. Schmidt, F. Zimmer, and S. Magalhaes, Physica A: Statistical Mechanics and its Applications **438**, 416 (2015).
- [11] F. M. Zimmer, C. F. Silva, S. G. Magalhaes, and C. Lacroix, Phys. Rev. E **89**, 022120 (2014).
- [12] M. Schmidt, F. M. Zimmer, and S. G. Magalhaes, J. Phys.: Cond. Matter **29**, 165801 (2017).
- [13] M. Fujihala, X. G. Zheng, Y. Oohara, H. Morodomi, T. Kawae, A. Matsuo, and K. Kindo Phys. Rev. B **85**, 012402 (2012).
- [14] K. Vijayanandhini, C. Simon, V. Pralong, V. Caignaert, and B. Raveau, Phys. Rev. B **79**, 224407 (2009).
- [15] E. V. Sampathkumaran, K. K. Iyer. S. K. Upadhyay, and A. V. Andreev, Solid State Communications **288**, 64 (2019).
- [16] R. Monasson and R. Zecchina, Phys. Rev. E **56**, 1357 (1997).
- [17] R. Erichsen and W. K. Theumann, Phys. Rev. E **83**, 061126 (2011).
- [18] C. Kwon and D. J. Thouless, Phys. Rev. B **43**, 8379 (1991).

- [19] Mézard, M. and Parisi, G., Eur. Phys. J. B **20**, 217 (2001).
- [20] R. Monasson, Journal of Physics A: Mathematical and General **31**, 513 (1998).
- [21] R. Abou-Chacra, D. J. Thouless, and P. W. Anderson, Journal of Physics C: Solid State Physics **6**, 1734 (1973).
- [22] R. Pohle, O. Benton, and L. D. C. Jaubert, Phys. Rev. B **94**, 014429 (2016).
- [23] C. F. Silva, F. M. Zimmer, S. G. Magalhaes, and C. Lacroix, Phys. Rev. E **86**, 051104 (2012).
- [24] N. Schupper and N. M. Shnerb, Phys. Rev. E **72**, 046107, (2005).
- [25] C. A. Morais, M. J. Lazo, F. M. Zimmer, and S. G. Magalhaes, Phys. Rev. E **85**, 031113 (2012).

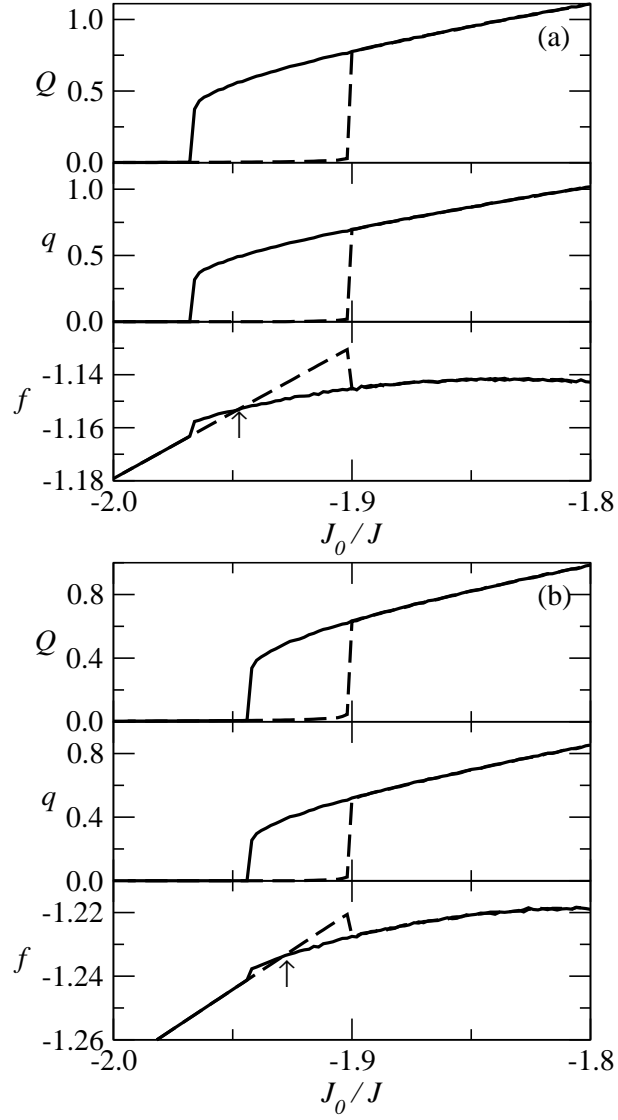


FIG. 7. (a) Total spin of the cluster Q , CSG order parameter q and free energy f vs. J_0/J for $T/J = 0.10$ and $c = 8$. (b) The same, but for $T/J = 0.15$. Solid (dashed) lines indicate heating (cooling). The arrows indicate the loci of the discontinuous transitions.

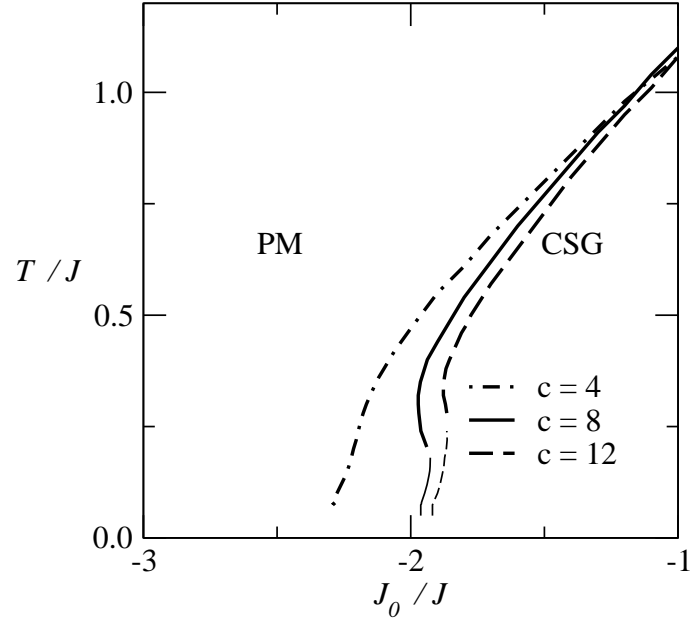


FIG. 8. T/J vs. J_0/J phase diagrams in clusters of regular tetrahedrons for $c = 4$, $c = 8$ and $c = 12$. Thin lines represent first order phase transitions.